

pubs.acs.org/acsapm Article

Temperature-Responsive Structurally Colored Fibers via Blend Electrospinning

Melissa W. Williams, James Aaron Wimberly, Ratib M. Stwodah, Jimmy Nguyen, Paola A. D'Angelo, and Christina Tang*



Cite This: ACS Appl. Polym. Mater. 2023, 5, 3065-3078



ACCESS

Metrics & More

Article Recommendations

Supporting Information

ABSTRACT: Achieving fibers that change color with temperature may be promising for applications such as sensors and smart wearable textiles (woven and nonwoven). In this study, temperature-responsive cholesteryl ester liquid crystal formulations were blended with polycaprolactone or polystyrene using chloroform as a solvent for electrospinning to achieve thermochromic nonwoven products. Using polystyrene, beaded fibers were achieved and the thermochromic behavior was only observed under polarized light microscopy. To achieve fibers with visible thermochromic behavior observed by a video



camera or smart phone, polycaprolactone was used as a carrier polymer. The comparison between polystyrene and polycaprolactone provides insight into polymer/solvent selection achieving responsive materials via blend processing. High loadings of liquid crystal were achieved with polycaprolactone, blends of 10 wt % polycaprolactone with 15 wt % liquid crystal formed fibers (fiber contained 60 wt % liquid crystal). Colored fibers could be achieved by varying the formulation of the liquid crystal. For example, liquid crystal formulations that were green at ambient conditions resulted in fibers that were green at ambient conditions (22 °C). Nonwoven fibers with dynamic color with temperature were also demonstrated. For example, liquid crystal formulations were colorless at ambient conditions and underwent a reversible color change from red to blue when heated and cooled between 32 and 37 °C. When incorporated into fibers, the fiber mats changed from white at ambient conditions to red at 32 °C to blue at 37 °C. The color change was reversible over multiple cycles.

KEYWORDS: electrospinning, smart fiber, liquid crystal, thermochromic, structural color

■ INTRODUCTION

Smart, responsive fibers have many potential applications in health care, personal protection, etc. 1,2 A wide range of materials that undergo reversible physical/chemical change in their properties upon exposure to light, magnetic fields, electricity, temperature, pH, and chemical stimuli have been studied and incorporated into fibers for soft robotic and sensing applications. 1,3,4 Such fibers, their fabrication, and their applications have been recently reviewed elsewhere. 1,5 Fibers on the order of $10-100 \ \mu m^1$ can be woven⁶ or knit into traditional textiles. For example, temperature-responsive fibers have been achieved by coating black filament with thermochromic liquid crystals.^{6,7} The \sim 100 μ m fibers could then be woven or knit into larger structures.^{6,7} Reducing fiber size can enhance the dynamic properties of the responsive materials (e.g., response time). Electrospinning is a versatile approach to achieving smart fibers (nanofiber to micron). The reduced diameter and higher specific surface area can facilitate interactions with the external environment and high sensitivity.1 Furthermore, electrospinning has enabled use of inorganic and organic functional materials. 1,8 Advanced fiber structures, e.g., porous and hollow fibers, coaxial and triaxial fibers, and Janus fibers with various capabilities, have also been

demonstrated.^{8–10} Commercial products based on electrospun fibers have included filters, masks, and wound dressings.¹¹

Electrospinning temperature-responsive fibers could enable innovative face mask design, ¹² e.g., color change indicator of respirator fit ¹³ or fever ¹⁴ based on changes in temperature. Thermotropic liquid crystals (LCs) have been widely used in temperature indicators based on visual observation of their structural color. ^{15,16} Their temperature-dependent structural color arises from the molecular, helical structure of the cholesteric phase with a temperature-dependent pitch length. ^{15,16} When the pitch length is on the order of the wavelength of visible light, the LC phase reflects visible light due to Bragg reflection ^{17,18} leading to strong iridescent color. ¹⁹ Changes in temperature result in twisting and untwisting of the helical structure resulting in reversible changes in the pitch length and thus the reflected color. However, electrospun fiber mats are highly scattering due to the many interfaces, which

Received: February 3, 2023 Accepted: March 21, 2023 Published: March 30, 2023





© 2023 American Chemical Society

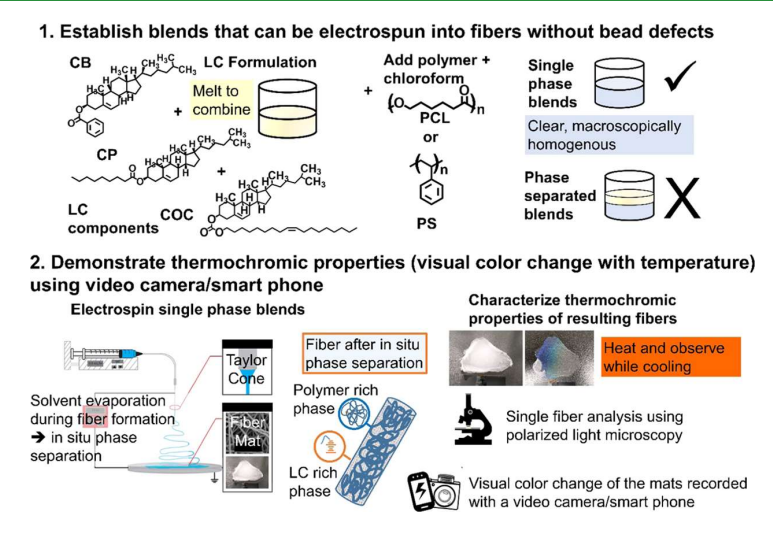


Figure 1. Overview of the preparation and characterization of thermochromic polymer/LC fibers using PCL or PS.

can affect the visual appearance of electrospun fibers containing thermochromic material. Thus, achieving thermochromic nonwoven products with visible dynamic color remains an important challenge toward producing functional stimuli-responsive materials (e.g., color-changing masks for fever detection). The goal of this work is to incorporate thermotropic liquid crystals into electrospun fibers and demonstrate visual observation of their dynamic color using a video camera/smart phone.

LCs have been successfully incorporated into polymer fibers via electrospinning. Coaxial electrospinning has been used to encapsulate LC in core-shell fiber cores. 20-23 For example, nematic LCs such as MBBA, ²⁴ E7, ²³ 5CB, ^{20,22,23,25,26} mixtures of nematic LCs with a chiral dopant, 27-30 and have been coaxially electrospun with a poly(vinyl pyrrolidone) (PVP) shell. Cholesteric LCs have also been coaxially electrospun with a PVP shell and the individual fibers colored when viewed under polarized light microscopy, but the visible color of the fiber mat was not demonstrated.³⁰ Further, the scale-up of coaxial electrospinning is more complex than single-needle electrospinning due to the multiple solutions in separate layers.^{9,31} So, although there have been many commercial products based on single-needle electrospinning, no coresheath fiber products have been commercialized to date.^{9,31} Alternatively, blend electrospinning (co-electrospinning) in which the LC can be dissolved with a polymeric solution for electrospinning from a single needle can be used to incorporate LC in polymer fibers.³² In blend processing, the polymer and LC can be combined in a common solvent. 19,33,34 Upon processing and solvent evaporation, phase separation of the polymer and LC occurs during fiber formation and the resulting fiber contains LC domains dispersed in a polymer matrix. 19,33,34 For example, various liquid crystal polymer blends 5CB, 6CB, or 7CB blended with PAN in DMF. 35,36 The resulting fibers show birefringence and may be useful for lightmodulating devices.³⁶ Chiral dopant R5011/PVA bends in DMF/H₂O have been electrospun and used to modulate the reflectance properties of LC devices.³⁷ Using blend electrospinning, cholesteric LCs incorporated in PCL fibers were visibly colored at a fixed temperature.³⁸ However, the

thermochromic response was not investigated³⁸ and the dynamic color of the fibers has not been established.

Overall, the focus of this work was (1) establishing electrospinnable polymer/LC blends using single-needle electrospinning and (2) demonstrating the visual dynamic color of the resulting nonwoven fibers observed with a video camera/smart phone. In this study, cholesteryl ester-based LCs were blended with PCL or PS. The appropriate polymer concentration and ratio of LC to polymer to achieve fibers without bead defects were investigated. The effect of fiber processing on the resulting thermochromic properties was investigated. The thermochromic properties of the individual fibers and fiber mats were demonstrated and compared. The reversibility of the visible color change was examined.

MATERIALS AND METHODS

Materials. Polycaprolactone (PCL) (molecular weight (number average) = 80,000 g/mole, ≥99.5% purity) and polystyrene (PS) (molecular weight (number average) = 170,000 g/mol), >95% purity were obtained from Sigma-Aldrich (St. Louis, MO). Chloroform (ACS reagent grade, ≥99.8% purity) was obtained from Fisher Scientific (St. Louis, MO). Cholesteryl oleyl carbonate (COC, quality level 100 (purity not specified)) and cholesteryl benzoate (CB, 98% purity) was obtained from Sigma-Aldrich (St. Louis, MO); cholesteryl pelargonate (CP) was obtained from either Sigma-Aldrich (St. Louis, MO, 97% purity) or Alfa Aesar (Ward Hill, MA, >95% purity). All materials were used as received.

Liquid Crystal (LC) Formulation. Thermochromic LCs were formulated based on previous reports. ^{30,39} Briefly, ternary mixtures of cholesteryl oleyl carbonate (COC), cholesteryl benzoate (CB), and cholesteryl pelargonate (CP) were combined at ambient conditions. The components were heated in an oil bath at 80-90 °C for 20 min to fully melt the components (Figure 1). Upon melting, the resulting blends were clear and macroscopically homogeneous. The LC formulation was cooled to ambient conditions before further use. Three different compositions were made based on previous studies; the composition affects the thermochromic behavior. At constant CB concentration, varying the ratio of COC to CP impacts the mesophase transition temperature and the resulting temperature at which color is observed.³⁹ Thermochromic behavior (color transitions between blue and red upon cooling) were expected to begin between 25, 30, and 43 °C for LC-1 (60 wt % COC/30 wt % CP/10 wt % CB), LC-2 (45 wt % COC/45 wt % CP/10 wt % CB), and LC-3 (30 wt % COC/60 wt % CP/10 wt % CB), respectively.3

depress the color transition temperature so that LC formulation appeared colored at ambient conditions, the COC content was increased to 80 wt % COC at constant CB concentration. Overall, the formulation was 80 wt % COC/10 wt % CP/10 wt % CB.

Electrospinning. For electrospinning, blends of polymer and LC were prepared by combining the solid polymer with the LC formulation at ambient conditions in various mass ratios. Chloroform was then added. Typically, the polymer concentration was 5–25 wt % and the LC formulation was 0–30 wt % of the total blend. The blends were stirred overnight (18–30 h) at ambient conditions until macroscopically homogeneous before electrospinning. Samples were stored at room temperature before further use. All samples were used within 1 week of preparation.

Electrospinning was performed using a point-plate configuration in which the polymer/LC blend was loaded into a syringe fitted with a stainless-steel needle (0.508 mm I.D.) and attached to a power supply (Matsusada Precision, Inc., model AU-40R0.75 with positive polarity). The blend was pumped at a flow rate of 0.5 mL/h using New Era Pump Systems syringe pump NE-300. Typical, spinning parameters were a tip-to-collector distance of 10 cm and applied voltage (positive polarity) of 7 kV. Electrospinning was performed at ambient conditions, i.e., temperatures between 19 and 23 °C, and relative humidity between 10 and 45%. Fibers were spun onto glass coverslips for analysis by PLM. Electrospinning was performed for 1 to 2 h to obtain samples that were sufficiently thick enough to remove from the foil for video analysis. An overview of the blend preparation, electrospinning, and fiber mat characterization is provided in Figure 1.

Fiber Characterization. Polarized Light Microscopy (PLM). The structure and thermochromic properties of the electrospun fibers were investigated using polarized light microscopy (PLM) (Nikon Instruments, Inc.) Eclipse 150N with Epi Rotatable Polarizer; L-AN analyzer with CFI60-2 TU Plan FLUOR BD objective lenses. To characterize the thermochromic properties, a microscope stage heater (Bioscience Tools, nominal accuracy of 0.1 °C) was used to heat the fiber samples which were electrospun onto glass coverslips placed onto the heat stage to 55 °C and held for 15 min at that temperature monitored with a thermocouple. Videos were recorded at 30 frames/s, using a DS-Fi3 (Nikon Instruments, Inc.) (2880 × 2048 pixels) as the sample was cooled to ambient conditions (68–74 °F/20–23 °C) under polarized light.

Scanning Electron Microscopy. Further analysis of the fiber structure was performed with scanning electron microscopy (SEM) (Hitachi Ultra High-Resolution Analytical FE-SEM SU-70) at 5 kV accelerating voltage at a 15 mm working distance. Fiber samples spun on aluminum were prepared for SEM analysis by sputter coating with carbon using a Denton Vacuum Desk V TSC JP Cold Sputtering Platform under 5×10^{-2} Torr pressure and at 75 amps for 1-2 s. The average diameter of fibers for each sample was determined from 100 measurements with ImageJ software (U.S. NIH).

DSC. Physically, the LC was expected to change color due to the Smectic A to twisted nematic phase transition. This mesophase transition temperature was measured using differential scanning calorimetry (Q100, TA Instruments). Samples were prepared by placing 4 to 6 mg samples of fibers containing LC into aluminum sample pans. An empty sample pan was used as a reference. To erase the previous thermal history and cool the sample to an initial "standard state", 40 the samples were first annealed by heating to 50 °C at a rate of 20 °C/min, held at 50 °C for 10 min, then cooled to -30 °C at a rate of 20 °C/min, and held isothermally for 15 min at -30 °C. These conditions were selected, so the mesophase transition temperatures could be compared to previous reports using the same procedure.³⁹ For analysis, the samples were heated from the initial standard state" of -30 to 70 °C at a rate of 10 °C/min based on previous analysis of PCL blends. 41 Based on the measured heat flow as a function of temperature, the endothermic melting peak ~25 to 30 °C attributed to the Smectic A to twisted nematic phase transition of the LC was determined using Universal Analysis 2000 software. Samples were prepared in triplicate; the average and standard deviation are reported as previously described.³⁰ The average value of

random error represents the accuracy of the results measuring the mesophase transition temperature of blends. 42

FTÎR Spectroscopy. PCL with and without LC were analyzed by Fourier transform infrared (FTIR) spectroscopy. Small sections of electrospun mats $(1 \times 2 \text{ cm}^2)$ were mounted onto a FTIR holder. Spectra were obtained using a Nicolet iS50 FT-IR spectrometer (Thermo Scientific) and analyzed with Omnic 9 software for FTIR.

UV-Vis Reflectance. To characterize the thermochromic behavior of the bulk fiber mats, 2×2 cm² sections were removed from the foil. The fiber mats were mounted on a black-coated, aluminum sheet. Fiber mats were then heated to 55 to 60 °C for 15 min. Samples were removed from the heat and analyzed as they cooled to ambient conditions (68-74 °F/20-23 °C) using ultraviolet-visible (UV-vis) reflectance spectroscopy. Specifically, UV-vis reflectance spectra (350-1200 nm) of the samples were obtained with an Ocean Optics (Largo, Fl.) Flame spectrometer (FLAME-S-VIS-NIR-ES) equipped with a tungsten-halogen light source (HL-2000-HP-FHSA, 20 W output) and a reflectance probe (RPH-1). The fiber mat was used as a reference. Measurements were taken every 10 s. Simultaneously, temperature measurements were taken with a thermocouple mounted near the fiber mat every 10 s HH802U Digital Thermometer with 800_multi_software for data logging (Omega Engineering, Stamford, CT). For each time point, wavelengths between 380 and 760 nm were further analyzed. The color corresponding to the reflectance spectra was defined using ISO 21348. The position of the leading peak was tracked as a function of time. The color transition temperatures (blue start, red start, red end) were determined as previously described.³⁵

Visual Analysis. Alternatively, as the samples cooled, the sample was viewed from a 90° viewing angle and video was recorded (Panasonic HC-V180 High-Definition video camera, 1920 \times 1080 pixels, 30 frames per second) for visual analysis. Frame-by-frame analysis was performed manually to estimate the color transition temperatures (blue start, red start, red end). Samples were prepared in triplicate; the average and standard deviation of the transition temperatures were reported.

From the video, freeze frames were selected and the color of the sample was analyzed. Specifically, chromaticity as a function of temperature was determined from the images. For a given frame, the RGB values of a given frame were obtained using a 40 \times 40-pixel area from the center of the fiber mat samples in ImageJ software. To quantify the perceived brightness of the colored sample in the image, the CIE Y value (a measure of luminance) was calculated using RGB values and eq 1

$$Y = 0.2162 R_{\text{linear}} + 0.7152 G_{\text{linear}} + 0.0722 B_{\text{linear}}$$
 (1)

The RGB values were then converted into Y_{xy} values using Python colormath. As Chromaticity plots were based on the CIE 1931 color space and using a 2° viewing angle and CIE D_{65} Standard Illuminant. 18,45

The reversibility of the color change was evaluated over multiple cycles. Four samples (1 × 2 cm² fiber mat) were removed from the foil and mounted on a black-coated, thin aluminum sheet. Fiber mats (PCL/LC-3) were heated to 55 to 60 °C, removed from the heat at allowed to cool to 28 °C, then reheated to 36 °C, and cooled repeatedly from 36 to 28 °C. Complete cycles, cooling then reheating, took approx. 6-7 min. Videos were recorded at a 90° viewing angle (Panasonic HC-V180, 30 frames per second) for visual analysis. Freeze frames (i.e., images) were taken from the videos as the samples cooled at expected blue start (36.5 °C) and red stop (33.5 °C) temperatures, and the color of the sample in the image was analyzed.³⁹ For a given frame, the RGB values of a given frame were obtained using a 40 × 40-pixel area from the center of the fiber mat samples in ImageJ software. The average RGB values were converted to CIE L*a*b* values using Python colormath. 43 Changes in chroma, calculated from a and b eq 2, 46 were monitored over multiple cycles. Chroma provided an indication of how dull or close to gray a color was. An increase in chroma or vividness represented color farther from gray.4

$$C^* = \sqrt{a^{*2} + b^{*2}} \tag{2}$$

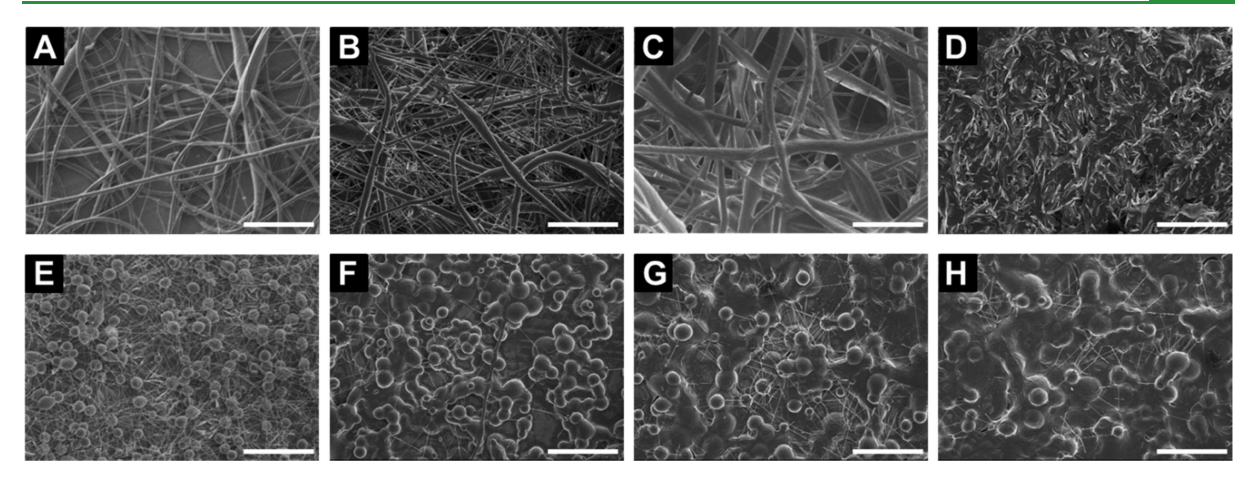


Figure 2. Effect of LC loading on PCL blends. The PCL concentration was held constant at 10 or 5 wt % while LC-3 loading was increased from ratios of 1:0 to 1:2 PCL/LC-3. (A) 10 wt % PCL/0 wt % LC, (B) 10 wt % PCL/10 wt % LC, (C) 10 wt % PCL/15 wt % LC, (D) 10 wt % PCL/20 wt % LC, (E) 5 wt % PCL/0 wt % LC, (F) 5 wt % PCL/5 wt % LC, (G) 5 wt % PCL/7.5 wt % LC, (H) 5 wt % LC/10 wt % LC. Scale bars are 100 μ m.

■ RESULTS AND DISCUSSION

Polymer/Liquid Crystal (LC) Blend Fiber Processing.

The goal of this work was to produce a nonwoven material that visibly changed color with temperature. Based on previous reports, LC formulations cannot be electrospun directly. Rather, the LC sprays into droplets when the electric field is applied.³⁰ LC has been incorporated into nonwoven fibers through coaxial electrospinning.³⁰ Color change in individual fibers was observed under a polarized light microscope.³⁰ However, visual color change of the resulting nonwoven fiber mat was not demonstrated. Furthermore, scale-up of coaxial electrospinning is more complex than single-needle electrospinning due to the multiple solutions in separate layers. 42 So, although there have been many commercial products based on single-needle electrospinning, no core-sheath fiber products have been commercialized to date. 9,42 Blending a material that cannot be electrospun (e.g., LC) with a polymer that can be electrospun has been a promising approach to achieve fibers from biopolymers for tissue engineering^{9,47} as well as reinforced composites^{9,48} using single-needle electrospinning^{9,47,48} Thus, the focus of this work was (1) establishing electrospinnable polymer/LC blends using single-needle electrospinning and (2) demonstrating the visual dynamic color of the resulting nonwoven fibers observed with a video camera/smart phone (overview, Figure 1).

In single-needle electrospinning of blends of polymer and liquid crystal (LC) from a common solvent, solvent evaporation during electrospinning can induce phase separation of the polymer and LC during fiber formation (Figure 1). ^{19,33,34} To perform single-needle electrospinning, a common solvent for the polymer and liquid crystal must be used and the composition of the blend is an important consideration. Chloroform was identified as an appropriate solvent for the liquid crystal formulation. ³⁸ Additionally, chloroform has previously been used in electrospinning polymer/LC blends and phase separation has been observed. ^{19,33,34} Next, polymers that could be electrospun from chloroform were identified. Both PCL ⁴⁹ and PS ⁵⁰ have been electrospun using chloroform as the solvent.

To establish electrospinnable polymer/LC blends using single-needle electrospinning, PCL or PS in chloroform were

used as carrier polymers. In electrospinning, a carrier polymer is a high-molecular-weight polymer that is blended with a material that cannot be directly electrospun. The polymer provides chain entanglement and can enable electrospinning. PS and PCL have been commonly used carrier polymers.

To start, electrospinning of PCL and PS in chloroform was briefly investigated. In electrospinning, the polymer concentration is an important consideration. In this work, the focus was investigating blend compositions (polymer concentration, LC-to-polymer ratio) that could be electrospun into uniform fibers at constant parameters. The tip-to-collector distance was held constant at 10 cm based on previous studies. 30,49,50 The flow rate was held constant at 0.5 mL/h. Lower flow rates led to a visibly beaded Taylor cone and beaded fibers (Figure S1): higher flow rates led to needle clogging. At a flow rate of 0.5 mL/h and a tip-to-collector distance of 10 cm, the voltage was varied to achieve electric field strengths between 0.1 and 1.5 kV/cm. Visual observations indicated that Taylor cones achieved electric field strengths at 0.7 kV/cm. Below this threshold, the electric field strength could not overcome the surface tension of the polymer solution resulting in needle clogging, which prevented uniform fiber formation. At higher electric field strengths, Taylor cones formed elongated droplets with multiple fiber strands at the needle tip, which produced beaded fibers. This procedure was consistent with previously established methods. 49 Based on this procedure, electrospinning process parameters including flow rate of 0.5 mL/h, tip-to-collector distance of 10 cm, and voltage of 7 kV at ambient temperature and humidity were used for electrospinning.

Using these process parameters, the polymer concentration that would produce uniform fibers was determined. For PCL, the concentration was varied from 1 to 18% and the effect of polymer concentration on fiber morphology was investigated. Beaded fibers were observed at 5 wt % PCL. With increasing concentration to greater than 10 wt % PCL, fibers without bead defects were achieved (Figure S2). This transition from beaded fibers to fibers without bead defects fibers has typically been attributed to polymer entanglement. ^{53,54} At low polymer concentrations, there are insufficient entanglements to with-

stand the stretching that occurs in the jet of fluid as it travels from the spinneret needle to the collector and it breaks apart into droplets as it travels. ^{53,54} Thus, a PCL concentration of 10 wt % was used to achieve fibers without bead defects. The effect of polystyrene (PS) concentration in chloroform on fiber morphology was also investigated. Beaded fibers were achieved at 5 wt % PS. With increasing PS concentration, fibers without bead defects were achieved at concentrations of 10 wt % PS and 15 wt % PS (Figure S3).

Next, blends of polymer (PCL or PS) and LC were investigated and the ratio of LC to polymer was studied. To introduce the LC formulations, compositions that formed single-phase blends (i.e., clear, macroscopically homogeneous mixtures of LC formulation and polymer) were examined. With increasing polymer and/or LC concentration, phase separation into a polymer-rich and solvent-rich phase can occur. Generally, phase separation was observed when total solids (polymer + LC) concentration was over 30–35 wt % for PCL blends and over 35–40 wt % for PS blends. Phase-separated blends were not further processed; single-phase blends were electrospun (Figure 1). PS blends and PCL blends that formed a single phase and were appropriate for electrospinning are summarized in the Supporting Information, Tables S1 and S2, respectively.

In order to establish polymer/LC blends that would electrospin and form fibers without bead defects, the effect of LC concentration at constant polymer concentration was examined using LC-3 as a model formulation. A polymer concentration with sufficient entanglement to spin fibers without bead defects was selected (i.e., 10 wt % PCL, Figure 2A). Introducing LC at a 1:1 PCL/LC ratio (by weight) did not significantly affect formation (Figure 2B). Further increasing the LC content to 1:1.5 PCL to LC by weight was possible without affecting the fiber quality (Figure 2C). As expected, increasing the solids concentration increased the fiber size. Specifically, the fiber diameter increased from 6.3 \pm 3.8 μ m for PCL alone to 13.4 \pm 13.7 μ m for the 1:1.5 PCL to LC-3 ratio (10 wt % PCL/15 wt % LC-3) (Table S3). Further increasing the LC content (i.e., 1:2 ratio of PCL to LC by weight) disrupted fiber formation and flake structures were observed rather than fibers (Figure 2D). Similar results were observed when adding LC to PS fibers. Higher LC loadings were possible using PS without disrupting fiber formation. Specifically, PS fibers without bead defects were achieved using 10 wt % PS. Fibers were achieved when LC was added to 10 wt % PS using LC content up to 1:3 PS/LC-3 by weight (Figure S4). Increasing the LC loading at constant 10 wt % PS concentration affected the fiber size. For example, the fiber size for 10 wt % PS spun alone was 5.7 \pm 3.5 μ m. Introducing 10 wt % LC loading (1:1 polymer/LC) loading increased the average fiber diameter to 16.6 \pm 8.1 μ m. Further increasing the LC loading to 30 wt % (1:3 polymer/LC) increased the average fiber diameter to 84 \pm 37 μ m (Table S3). Further increasing the LC loading resulted in phase separation of the blend prior to electrospinning and the blend could not be spun. Based on these results, LC can be incorporated in electrospun fibers by adding it to 10 wt % PCL or PS (polymer concentrations that form fibers without defects) and both PCL and PS appear to be effective carrier polymers for

incorporating LC into electrospun fibers.

Nguyen et al.³⁰ previously reported that introducing LC to beaded PS-only fibers improved the uniformity. Thus, the effect of LC concentration in the blend at a lower polymer

concentration was also examined. Polymer concentrations that produced beaded fibers when electrospun alone (i.e., 5 wt % PCL and 5 wt % PS) were selected. For example, 5 wt % PCL formed fibers with beads when electrospun from chloroform (Figure 2E) and LC was added. Introducing LC up to 1:2 by weight did not improve uniformity and only beaded structures were obtained from 5 wt % PCL blends containing LC (Figure 2F-H) (blend compositions tabulated in Table S2). Similar results were observed with PS. At 5 wt % PS, bead-on-a-string morphologies were observed and the surface of the beads appeared wrinkled (Figure S5). Similar morphologies have been previously reported and attributed to solvent evaporation during electrospinning. Upon introducing LC, the linear density of bead defects appeared to increase up to LC loadings of 1:5 PS/LC. With further increases in LC concentration (1:6 PS/LC) a transition from beaded fibers to flake-like structures outside the fiber (Figure S5). The effect of LC concentration at both 10 wt % polymer and 5 wt % polymer results further supports the observation that when using chloroform as the solvent, PCL and PS act as carrier polymers for the LC formulation. The carrier polymer is blended with a material (LC in this case) that cannot be directly electrospun and provides chain entanglement to facilitate fiber formation.⁵¹, Based on these results, for polymer/LC blend preparation, the polymer concentration in the solvent (common with the LC formulation) must be sufficient to form fibers without bead defects to provide sufficient molecular entanglement to act as a carrier polymer. 51,52 These results are consistent with using carrier polymers to electrospin conductive materials⁵¹ as well as proteins and polysaccharides.4

To confirm that the LC was incorporated into the fibers, FTIR spectroscopy of the electrospun PCL and PCL/LC-3 fiber mats was performed (Figure 3). PCL had a double peak

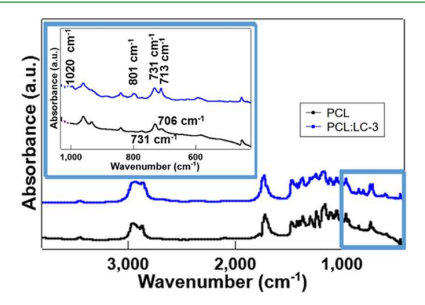


Figure 3. FTIR spectra of PCL (black) and PCL/LC-3 (blue). The inset highlights the differences between PCL/LC-3 and PCL.

at 2970 and 2960 cm⁻¹ representing asymmetric and symmetric stretching of CH₂, respectively.⁵⁵ PCL/LC-3 also had a double peak in this range, but the second peak was shifted slightly to 2940 cm⁻¹, which can be attributed to the presence of the LC.⁵⁶ A shoulder peak was also observed at 1764 cm⁻¹ for PCL alone and may be attributed to the carbonyl stretching of the amorphous portion of the PCL.^{41,57} Upon blending with LC, the shoulder is indistinct from the peak at 1720 cm⁻¹. Shifts to lower wavenumbers in PCL blends have been attributed to hydrogen bonding between the PCL chain and hydroxyl groups (of the LC components).^{41,57} Additionally, upon addition of the LC formulation, additional peaks were noted in the PCL/LC sample that were not seen in the PCL-only sample at 1020 and 801 cm⁻¹. Further, an increase of intensity and shift in one of the double PCL peaks

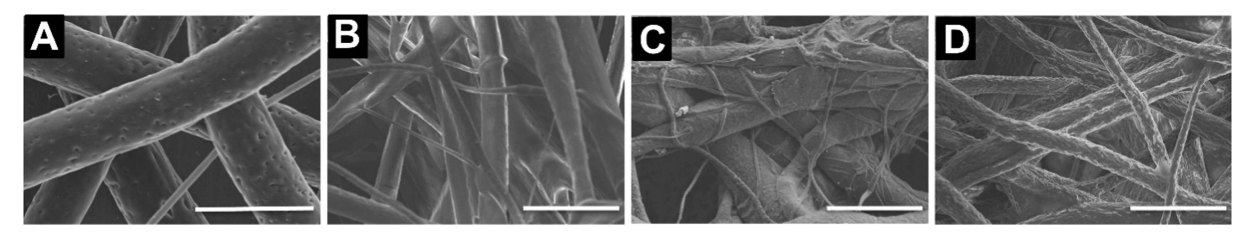


Figure 4. SEM images of electrospun fibers PCL fibers with various LC formulations. (A) 10 wt % PCL (10 μ m scale bar), (B) 10 wt % PCL/LC-1 (50 μ m scale bar), (C) 10 wt % PCL/LC-2 (50 μ m scale bar), (D) 10 wt % PCL/LC-3 (50 μ m scale bar).

(731/706 cm⁻¹) to 731/713 cm⁻¹ was observed. Peaks in this region can most likely be attributed to nonplanar bonding of ring-associated C–H bonds, which have been noted for CP. Since PCL has no ringed structures, the additional peaks can be attributed to the LC-3 blend of COC, CP, and CB and suggest the presence of LC in the polymer/LC blend fibers. The results (presence of LC peaks) are consistent with previous reports of electrospun blends of PAN and 7CB. ³⁵

Building on these results, the effect of LC formulation on electrospinning to vary the thermochromic properties of the resulting fibers was investigated. The focus of this work was to achieve fibers with comparable fiber size with different LC formulations. The observed color change for a set of samples at a constant polymer-to-LC ratio and comparable fiber properties could be compared to understand the effect of the LC ratio on the dynamic color. The observed color change in the fiber could be compared to the LC alone to understand the effect of the fiber structure on dynamic color.

Thus, the PCL and LC concentration was held constant at 10 wt % PCL and 15 wt % LC and blends were prepared with three different LC formulations (summarized in Table S2). The different LC formulations contain a constant amount of CB (10 wt %) and various ratios of COC/CP to tune the thermochromic properties. 39 The LC formulations were prepared first and then blended with the polymer and chloroform (Figure 1). In the electrospinning blends with the different formulations, the total solid (polymer + LC) concentration was held constant similar to other studies of electrospinning multicomponent blends. 59-61 SEM images of the three different LC formulations: LC-1, LC-2, and LC-3 are shown in Figure 4B-D. Based on the SEM images, the fibers were free from bead defects. The surface roughness of the fibers is consistent with other polymer/LC blend fibers and was considered an indication of in situ phase separation.³³ Average fiber diameters for 10 wt % PCL/15 wt % LC with the different LC formulations were comparable (Table 1).

The fiber size distributions compared to 10 wt % PCL are shown in the Supporting Information (Figure S6). As seen in the fiber size distributions, the largest fiber diameters observed on the SEM were $70-90~\mu m$ (Table S4), while the majority of fibers were less than 30 μm in diameter. With the 10 wt %

Table 1. Effect of LC Formulation on Fiber Diameter for 10 wt % PCL/15 wt % LC Samples^a

electrospun blend	fiber diameter (μ m) (ave. \pm std. dev.)
10 wt % PCL/15 wt % LC-1	14 ± 12
10 wt % PCL/15 wt % LC-2	13 ± 11
10 wt % PCL/15 wt % LC-3	13 ± 14

^aUsing PCL and an LC-to-polymer ratio of 1.5:1, the average fiber diameters were comparable for the different blends.

PCL/15 wt % LC blends, the LC formulations could be varied with comparable fiber properties. The observed color change for this set of samples at a constant polymer-to-LC ratio and comparable fiber properties could be examined to understand the effect of the LC composition on the dynamic color. The observed color change in the fiber could be compared to the LC alone to understand the effect of the fiber structure on dynamic color.

For PS, the highest LC loading that could be achieved while achieving uniform fibers was 10 wt % PS and 30 wt % LC-3. Thus, the PCL and LC concentration was held constant at 10 wt % PS and 30 wt % LC, and blends were prepared with three different LC formulations. All three LC formulations formed uniform fibers generally free of bead defects (Figure S7). The fiber size distributions for the 10 wt % PS and 30 wt % LC samples with LC-1, LC-2, and LC-3 compared (Figure S8) to 10 wt % PS are provided in the Supporting Information (Figure S8). With a 3:1 ratio of LC/PS, the fiber size in all three cases was larger than polystyrene alone. This increase in fiber size is expected when increasing the total solids concentration from 10 wt % with PS alone to 40 wt % (PS + LC). Examining the effect of LC formulation on fiber size, LC-1 (at the same concentration) had the smallest fibers and lowest coefficient of variation compared to LC-2 and LC-3, whereas LC-3 had the highest values (i.e., broadest fiber size distribution) (Table S5). These results indicate that increasing the CP content in the fiber (LC-3 has the highest CP content) increases the fiber diameter in PS/LC fibers spun from chloroform (Figure S9). In contrast, in the PCL/LC fibers, the LC formulation did not significantly affect fiber size. The ratio of LC to polymer was higher in the PS system (3:1 for PS compared to 1.5:1 for PCL); thus, the effect of LC formulation on size may also be affected by polymer as well as LC-topolymer ratio. In this work, comparing the thermochromic properties of 10 wt % PCL/15 wt % LC fibers using different LC composition would be especially valuable for physically understanding the role of processing the LC formulations into fibers on the observed properties since the fiber sizes are comparable.

A potential disadvantage of using carrier polymers is that the resulting fibers may not show the desired functional properties, in this case, thermochromic properties of the LC. ^{30,51} Thus, the focus of this work was establishing polymer/LC blends that could be electrospun into fibers without bead defects and demonstrating the visual color change of the resulting nonwoven fiber mats. Since blends using 10 wt % PCL and all three different formulations could be electrospun into fibers generally free of bead defects at constant LC content and comparable fiber properties, these samples were further analyzed. The observed color change for a set of samples at a constant polymer-to-LC ratio and comparable fiber proper-

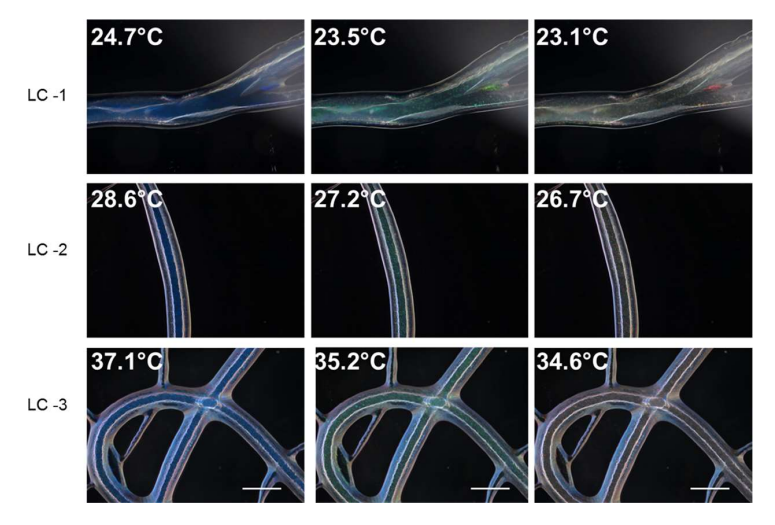


Figure 5. Polarized optical light microscopy (PLM) images of 10 wt % PCL/15 wt % LC for LC-1, LC-2, and LC-3 formulations. Samples were heated and imaged upon cooling to ambient conditions. Blue to green to red color transition was observed for all LC formulations as temperature decreased. Scale bars are 200 μ m.

ties could be compared to understand the effect of the LC composition on the dynamic color. The observed color change in the fiber could be compared to the LC alone to understand the effect of the fiber structure on dynamic color.

Thermochromic Characterization of Fibers. The thermochromic properties of the electrospun fibers were investigated. A summary of the fiber blends selected for thermochromic characterization based on the electrospinning results is provided in Table S6. As an initial indication of thermochromic properties, polarized light microscopy (PLM) was used to observe the resulting fibers (single fiber analysis). The fibers were heated to 55 °C (above the expected mesophase transition temperature)³⁹ and observed as the fibers cooled to ambient conditions. Upon cooling, a color transition was observed in the 10 wt % PCL and 15 wt % LC fibers from blue to red for all LC blends (Figure 5). This color transition can be attributed to the LC, specifically the Smectic A to twisted nematic (SA*-N*) phase transition. 39 Specifically, at higher temperatures, the LC helical coil tightened so that the pitch is shorter. The shorter pitch caused the polarized light from the microscope to selectively reflect shorter wavelengths in the blue range. As the fiber continued to cool, the helix relaxed more so that longer wavelengths were reflected; thus, green and red and finally out of the visible spectrum (colorless) were observed (Figure 5). The blueshift upon heating due to pitch contraction has been attributed to a "pretransition" in which the Smectic A and twisted nematic (or chiral) phases are mixed near the mesophase transition. In the "pretransition" mixed phase, the pitch of the CLC is effectively infinite and contracts to finite values resulting in an apparent blueshift. 16 The color change with temperature that was observed was intrinsic to the liquid crystal formulation (i.e., helical twisting power of the chiral component(s)). 16 Interestingly, the color change under PLM was observed to be uniform in contrast to previous reports using coaxial electrospinning in which fiber diameter caused slight differences in inherent pitch lengths because of radial confinement.⁶² This result was notable because LC incorporated into electrospun fibers via coaxial electrospinning has been previously observed, and no color change was observed in

fibers prepared via blend electrospinning of PS/LC from a toluene/acetone solvent mixture. 30

For 10 wt % PS, 30 wt % LC (as well as 10 wt % PS, 15 wt % LC), no thermochromic behavior using PLM was observed (Figures S10 and S11). These results were consistent with previous reports blend electrospinning with liquid crystal.³⁰ Interestingly, at lower polymer concentrations and higher LC content 5 wt % PS, 25 wt % LC when the fibers were heated to 55 °C and observed as the fibers cooled to ambient conditions, a color transition from blue to red was observed (Figure S12). There were several differences between the results presented here using 5 wt % PS/25 wt % LC (thermochromic) and 20 wt % PS/20 wt % LC (no thermochromic behavior observed under polarized light microscopy). The liquid crystal-topolymer ratio was 5:1 compared to 1:1. Another important difference was the volatility of the solvent:chloroform compared to toluene/acetone. In a polymer blend, the phase morphology can be affected both by the rate of solvent evaporation and by the blend composition. 63 Both a higher LC/polymer ratio and more volatile solvent would promote in situ phase separation during fiber formation.⁶³ Such phase separation may be important to maintaining the thermochromic properties of the LC in the electrospun fiber. Another difference between 5 wt % PS/25 wt % LC (thermochromic) and 20 wt % PS/20 wt % LC (no thermochromic behavior observed under polarized light microscopy) is the fiber morphology. The 5 wt % PS/25 wt % LC electrospun from chloroform fibers had bead defects, whereas the 20 wt % PS/20 wt % LC electrospun from toluene/acetone did not have bead defects. For electrospun fibers, both fiber size⁶⁴ and fiber spacing⁶⁵ have been shown to affect reflectance properties due to interfiber and inner-fiber scattering. Thus, the difference in fiber morphology may also impact the apparent thermochromic properties. Leveraging the fiber mat structure to further tune the thermochromic properties may be possible. In this work, the focus was on the effect of LC formulation in fibers without bead defects.

With PS as the polymer, using a polymer concentration high enough to produce fibers without defect resulted in fibers that did not show thermochromic properties. This result suggests that PS entanglement may affect the apparent thermochromic properties of the resulting blend fibers. Further, comparing PS/ LC fibers to PCL/LC fibers at 10 wt % fibers without bead defects, no color transitions were observed in the PS fibers, whereas color transitions were observed in the PCL fibers. The lack of color transitions for PS a may have to do with the lower chain mobility of PS, as indicated by its high glass-transition temperature, $T_g = 95$ °C, 66 in contrast to PCL, with a T_g of -60 °C. 67 Anisotropic LC interactions with PS (vinyl chain vs side chains) may also affect the LC assembly⁶⁸ and the resulting thermochromic properties. Practically, when using PS, there is a trade-off between achieving bead-defect-free fibers and thermochromic behavior. The 10 wt % PCL, 15 wt % LC blends were the only system that appeared to form fibers without bead defects with thermochromic properties observed on the PLM. Overall, selecting a polymer electrospinnability in a solvent that is miscible with the LC formulation and low glass-transition temperature appears to be important considerations for blend electrospinning.

For quantitative evaluation of the thermochromic properties of the 10 wt % PCL, 15 wt % LC fibers, frame-by-frame video analysis was performed manually to determine the (1) blue start, (2) red start, and (3) red end transition temperatures. These color transition temperatures for the fibers containing the different LC formulations are summarized in Table S2. For example, for 10 wt % PCL/15 wt % LC-3, the blue start temperature was 36.9 ± 0.6 °C, the green start temperature was 33.9 \pm 0.6 °C, and the red end temperature was 32.0 \pm 0.5 °C. The start of the color transition (i.e., the blue start temperature) for the three formulations is slightly above the mesophase transition temperature of the LC in the fiber measured by DSC. For example, for 10 wt % PCL/15 wt % LC-3, the blue start temperature was 36.9 ± 0.6 °C and the mesophase transition temperature of the LC in the fiber measured by DSC was $35.\overline{1} \pm 0.1$ °C (Table S7). This result was expected because the thermochromic behavior occurs physically due to Smectic A to the twisted nematic phase transition (measured by DSC).⁶⁹ Similar results were observed with the LC alone.39

Interestingly, the mesophase transition temperature for the LC in the PCL fibers was comparable to the LC alone (Table S7).³⁹ For example, the mesophase transition temperature of LC-3 alone was 36.1 \pm 0.1 °C, and that for LC-3 in the 10 wt % PCL/15 wt % LC fiber was 35.1 ± 0.1 °C (Table S2). This result indicates that fiber processing and confinement within the polymer fiber did not significantly affect the transition temperature. In contrast, the clearing point of nematic LCs has shifted significantly (e.g., 15 K compared to the bulk LC) when incorporated into coaxially electrospun fibers.^{24,62} The effect has been modulated by the presence of surfactants in the PVP electrospinning solution.²⁵ The presence of surfactant at the LC polymer interface was thought to affect LC alignment and ultimately the energy required for the phase transition.²⁵ cholesteric phase transition may be less affected than the nematic transition. Additionally, blend electrospinning may affect the phase transition less than coaxial electrospinning which typically involves a nonsolvent for the LC. Importantly, the phase behavior of the LC in the polymer/LC blend fiber can be predicted by the behavior of the LC formulation, an important practical consideration when formulating and processing blends for product development.

Thermochromic Characterization of Fiber Mats. When incorporating cholesteric LCs into electrospun fibers, temper-

ature-dependent iridescent properties have been observed in single fibers using PLM.⁶² However, mats of the fibers have been considered highly scattering due to the many interfaces.⁶ Thus, achieving thermochromic nonwoven products with visible dynamic color remains an important challenge toward producing functional stimuli-responsive materials (e.g., color-changing masks for fever detection). Thus, the focus of this work was to visualize the color change of the nonwoven fiber mats using a video camera or smart phone without specialized equipment (i.e., microscopes, polarizers).

Sections of fiber mats were mounted on a black-coated, thin aluminum sheet and heated to 55 to 60 °C (above the mesophase transition temperature of the LC). The sample was observed as it cooled to ambient conditions; videos were recorded at a 90° viewing angle. As fiber mats cooled, fiber mats transitioned from bright purple color, to blue, green, yellow, orange, red (Figure 6A), and back to colorless/white.

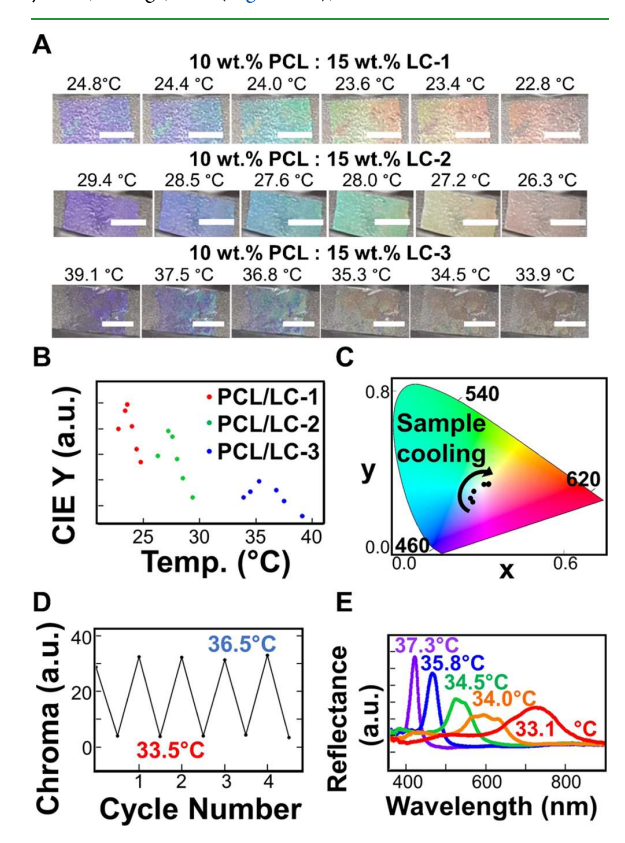


Figure 6. (A) Visual analysis of 10 wt % PCL/15 wt % LC fiber mats demonstrating thermochromic properties. Samples were heated and video recorded as they cooled to ambient conditions. Representative images showing the color transitions from purple to red during cooling with a 1 cm scale bar. (B) From the images, CIE Y values as a function of temperature were calculated as a measure of perceived sample brightness. The CIE Y increases as the samples brightned in the blue region and then faded in the red region (intrinsic to the LC). (C) Representative chromaticity plot (CIE 1931) for PCL/LC-3 demonstrating the colors observed upon sample cooling (D) reversibility of the color change demonstrated by the chroma values for PCL/LC-3 at blue start, 36.5 °C, and red stop, 33.5 °C over multiple heating and cooling cycles (E) UV—vis reflectance spectra of PCL/LC-3 as the sample cooled. The reflectance peak shifted to higher wavelengths due to the transition from purple to red.

Slight variations in color across the sample from left to right can be observed and may be attributed to nonuniform heating (using a hot plate). Interestingly, colors observed during the color transition were visually brighter for LC-1 and LC-2 than for LC-3.

Based on the images, the differences in brightness between PCL/LC-1, PCL/LC-2, and PCL/LC-3 observed in the images were verified quantitatively by calculating the CIE Y value (a measure of relative luminance or perceived sample brightness) for PCL/LC fiber mats. As shown in Figure 6B, for all of the formulations, as the color transition occurred, there was an increase in the CIE Y value after the first color was observed. This observation is consistent with the LC alone.³ Levit et al. also reported that the LC samples brightened in the blue region and faded in the red region.³⁹ The increase in CIE Y corresponded to the LC initially increasing in brightness in the blue region, and then the CIE Y values decrease as the sample fades in the red region. Thus, the changes in CIE Y are likely intrinsic to the LC formulation visualized in a confined (tubular geometry). Also, the temperature of the color transition for the fiber mat was comparable to the LC alone and thus can be attributed to the mesophase transition temperatures of the LC formulations (Table S7). Further, as the COC content in the formulation decreased, the peak in CIE Y decreased and PCL/LC-1 showed the highest peak corresponding with the brightest appearing sample (Figure 6B). Thus, the quantitative assessment of perceived sample brightness matched the visual observations captured in the images (Figure 6A). In the videos, the same trend in CIE Y values for LC alone (i.e., the color transition was brighter for LC-2 than LC-3) was observed (Figure S13). Physically, color brightness of LCs is affected by the anisotropy of LC layers and samples with reduced brightness have lower reflective index differences between layers. 70 The different formulations may have different brightness due to the composition. COC has a bent cis-configuration with an alkene side chain that limits folding, whereas CP has a linear configuration. 71 The high the COC content (i.e., LC-1), the more layers the bent cisconfiguration introduces, and thus more the pitch anisotropy. As the ratio of the amount of COC is reduced and CP is increased, pitch anisotropy is increased, reducing brightness. The layering of the LC may be further affected by incorporation in PCL fibers. Interestingly, these visual observations were not consistent with observations made using PLM by Levit et al.³⁹ In contrast, Levit et al. observed that the color transition of LC-3 was brighter than LC-2. This difference can be attributed to the difference in method, i.e., visual observation under ambient lighting compared to observation under dark-field PLM. Specifically, viewing the samples using cross-polarizers increases the contrast between the colorless and brightest observed blue (Figure S13). This result demonstrates the importance of performing visual analysis in parallel with more specialized methods of analysis (e.g., PLM) as the findings may change. Performance using visual methods under ambient lighting conditions is important for practical applications.

Since the color transition was comparable, but most difficult to see (least bright) for LC-3, it was used for further analysis. Notably, the first color observed for the PCL/LC mats was purple compared to blue typically reported for the LC alone. ^{15,17,39} The visual observation (Figure 6A) was confirmed using a chromaticity diagram in International Commission of Illumination (CIE) 1931 color space ^{44,72} to

demonstrate the range of colors observed during cooling (Figure 6C). Representative images from the video analysis of PCL/LC-3 were analyzed and compared to representative images of LC-3 (Figure S14). The differences in perceived color between the color start and red end were quantified using the color difference (ΔE). 39,45 For PCL/LC-3, the calculated difference in perceived color in CIE $L^*A^*B^*$ color space between the color start and the red end was 29, whereas the difference for the LC-3 sample was only 12. This result indicates that the dynamic color (color start to red end) is more noticeable in the fibers than the LC formulation alone. 39,45

Additionally, the visually observed color changes (Figure 6A) were confirmed with UV-vis reflectance. As the sample cooled, the peak in reflected wavelength shifted from 380 to 760 nm. Representative changes in UV reflectance spectra as the sample cooled are shown in Figure 6E. For example, the reflectance peak in Figure 6F shifted from 422 nm at 37.3 °C (purple) to 465 nm at 35.8 °C (blue), to 525 nm at 34.5 °C (green), to 593 nm at 34.0 °C (orange), and to 703 nm at 33.1 °C (red). Colors are based on ISO 21348 definitions. The reflectance peaks decreased in intensity and broadened as the fiber mats cooled. Broadening of the reflection peak has been attributed to nonuniform pitch distribution of the LCs within multilayer polymer/LC system.⁷³ Nonuniform pitch distribution may be attributed to variations in fiber size as well as slight temperature gradients within the sample between the solid surface and the surface exposed to ambient conditions. The decreases in intensity are consistent with the observed decreases in brightness as the sample transitioned from blue to red. These results are comparable to the results reported for the LC alone.³⁹ The changes in UV reflectance are consistent with the observed color changes and are indicative of an increase in the helical pitch length of the LCs as the sample cooled. Despite the peak broadening and decreases in intensity, the color change is visible when observed using a video camera/smart phone.

Based on the video analysis, the color transition temperatures were estimated. The transition temperatures were compared to the transition temperatures measured by UV analysis, and the results with UV reflectance confirm visual results. For example, for LC-3 using visual analysis, the blue start temperature was 38.3 \pm 0.5 °C, the green start temperature was 35.2 \pm 1.3 °C, and the red end temperature was 33.0 ± 0.5 °C. Using UV reflectance, the blue start temperature was 36.9 ± 0.5 °C, the green start temperature was 33.8 \pm 1.3 °C, and the red end temperature was 33.2 \pm 0.4 °C. Slight discrepancies were observed for the blue start transition temperature, whereas no significant differences were observed in the red start and red end temperatures (Table S8). The slight difference may be attributed to the visual transition from purple to blue being more subtle than yellow to red or red to colorless. Further, the transition temperatures of the fiber mats were comparable to the single fibers. For example, using visual analysis of single PCL/LC-3 fibers under PLM, the blue start temperature was 36.9 ± 0.6 °C and the red end temperature was 32.0 \pm 0.5 °C (compared to a blue start of 36.9 ± 0.5 °C and the red end temperature was 33.2 ± 0.4 °C for the fiber mats). The observed differences are relatively minor (Tables S7 and S8) and may be attributed to structural differences between individual fibers and bulk fiber mats as mats are anisotropic and made up of a range of fiber diameters (Table S3), which is known to affect the color of the fiber. 16,26 The transition temperatures using UV analysis were used for further analysis of the thermochromic properties of the fiber mats, i.e., color transitions using "color bandwidth" and "color play" values. ^{17,39}

Bandwidth is the difference between the blue start (first occurrence of $\lambda_{\rm max}$ between 450 and 500) and red start (first occurrence of $\lambda_{\rm max}$ between 610 and 760 nm) temperatures. ^{17,39} Based on the UV reflectance measurements, the bandwidths for PCL/LC-1, PCL/LC-2, and PCL/LC-3 were 1.6 \pm 0.5, 2.4 \pm 0.32, and 2.2 \pm 0.6 °C, respectively. These values were the same (statistically) as the bandwidth values measured by Levit et al.: 2.5 \pm 1.4 °C for LC-2 alone and 2.3 \pm 1.6 °C for LC-3 (Student's *t*-test, α = 0.05).³⁹

The "color play" domain represents the entire temperature range of visible color, from the first appearance of color to its disappearance. The "color play" is affected by the intrinsic cholesteric pitch length and helical twisting power. The color play of the LC in the single fibers for LC-2 (3.9 \pm 0.6 °C) and LC-3 (4.9 \pm 0.8 °C) was comparable to previously reported values for the LC formulations (4.5 \pm 1.5 °C for bulk LC-2 and 6.1 \pm 1.6 °C for bulk LC-3); no statistical difference was observed using a Student's *t*-test, α = 0.05 (Table 2). This

Table 2. "Color Play" Analysis to Describe Thermochromic Properties of the Fiber Mat Compared to the Single Fiber and LC Alone

LC formulation	color play LC (°C) ³⁹	color play PCL/LC single fiber (°C)	color play PCL/LC fiber mat (°C)
LC-1	n/a	n/a	7.5 ± 0.7
LC-2	4.5 ± 1.5	3.9 ± 0.6	10.2 ± 0.9
LC-2	6.1 ± 1.6	4.9 ± 0.8	9.7 ± 1.1

result suggests that fiber processing and confinement within the fiber did not significantly affect the intrinsic cholesteric pitch length of the LC. In the case of PCL/LC fiber mats, "color play" was determined based on the UV reflectance measurements by finding the difference in temperatures between temperatures at purple start (i.e., first occurrence of λ_{max} between 360 and 450 nm) and red end (last occurrence of $\lambda_{\rm max}$ between 610 and 760 nm). Interestingly, the color play range for the mats was significantly wider, with 10.2 \pm 0.9 °C for PCL/LC-2 and 9.7 \pm 1.1 °C for PCL/LC-3, in contrast to UV values of 4.5 \pm 1.5 °C for bulk LC-2 and 6.1 \pm 1.6 °C for bulk LC-3 (Student's *t*-test, α = 0.05) (Table 2). ³⁹ Broadening of the color play region in the fiber mats may be ascribed to the layered, anisotropic configuration of the electrospun fibers. Several studies have found that layering of cholesteric LCs^{74,75} or natural cholesteric structures⁷⁶ of differing pitch has the effect of broadening the wavelength bandgap. Taken together, these results suggest that in the individual fibers, the intrinsic pitch length was not affected, and layering multiple fiber layers may affect the structural color and visual dynamic temperature response of the resulting fiber mats.

Taken together, the results indicated that the apparent thermochromic properties of the resulting nonwoven product can affect the structure of the mat. For electrospun fibers, both fiber size and mat thickness⁶⁴ as well as fiber spacing⁶⁵ have been shown to affect reflectance properties due to interfiber and inner-fib er scattering. Thus, it is possible that mat properties such as fiber size and mat thickness could be used to further tune the thermochromic properties of the resulting fiber mat. A careful design of experimental study to further

elucidate how to tune fiber size (processing parameters, blend composition, etc.) and the resulting optical properties of the resulting fiber mat (e.g., refs 77, 78) could be useful in product design as a future direction.

For practical applications such as temperature monitoring based on visual color detection, reversible color change can be important. SEM was performed after color change. Heating and cooling did not appear to significantly affect the fiber morphology (Figure S15). The average fiber size was also comparable: $13 \pm 14 \,\mu \text{m}$ (as spun) and $15 \pm 21 \,\mu \text{m}$ after color change. Thus, the reversibility of the thermochromic behavior of the fiber mats was investigated using visual detection. As proof of concept, 10 wt % PCL/15 wt % LC-3 was video recorded as it was heated, cooled, and reheated for multiple cycles. For analysis, chroma values were compared at the blue start temperature (36.5 °C) and red end temperature (33.5 °C) as a measure of the perceived color. 46 Chroma values decreased as the sample fades and turns from red to blue upon heating, and they increased as the sample brightens and turns from blue to red upon cooling. For example, at the blue start temperature (36.5 $^{\circ}$ C), the average chroma value was 31.5 \pm 1.7 over five cycles, and at the red end temperature (33.5 °C), the average chroma value was 4.0 ± 0.3 . The chroma values were consistent with multiple cycles (Figure 6D), indicating the color change (i.e., blue to red, as well as the changes in brightness) was repeatable over multiple heating and cooling cycles. This result demonstrated the changes in the helical pitch of the LC after fiber processing remained reversible. Thus, these materials could be used for temperature monitoring based on visual color detection, 46,80 e.g., smart masks for fever detection. 12–14

Using LC-1, LC-2, and LC-3, the fiber mat was white at room temperature; color appeared when the sample was heated (e.g., Figure 1). Achieving fibers that are structurally colored at room temperature has been of interest for avoiding fiber dying processes that produce significant amounts of wastewater. Thus, a proof-of-concept experiment to demonstrate structurally colored fibers at ambient conditions was investigated. The goal of this experiment was to achieve visually colored fibers at ambient conditions (captured with a smart phone camera). An LC formulation with a lower mesophase transition temperature so that the formulation appeared colored at ambient conditions was developed. Thus, the COC content in the formulation was increased while holding the CB concentration constant at 10 wt %. By increasing the COC content to 80 wt % (formulation 80 wt % COC, 10 wt % CP, 10 wt % CB), the resulting formulation was spread on a glass slide and appeared blue at ambient conditions (\sim 71 °F/22 °C) (Figure 7A). The nonuniform color may be attributed to differences in thickness when the sample was spread on the glass slide affecting the apparent local temperature of the LC at ambient conditions. In contrast, the other LC formulations were colorless or white at ambient conditions (Figure S16) and changed color when heated. Using this formulation, PCL/LC fibers using 10 wt % PCL/15 wt % LC were electrospun. Based on SEM, the fiber morphology was comparable and generally free of bead defects (Figure S17). The average fiber diameter was 17 \pm 13 μ m, comparable to the other electrospun PCL/LC fibers (Figure S17 and Table S4). The resulting fibers, in Figure 7B, were visibly colored (green) at ambient conditions (22 °C), consistent with the color of the LC formulation under comparable conditions. The slight variation in color may be

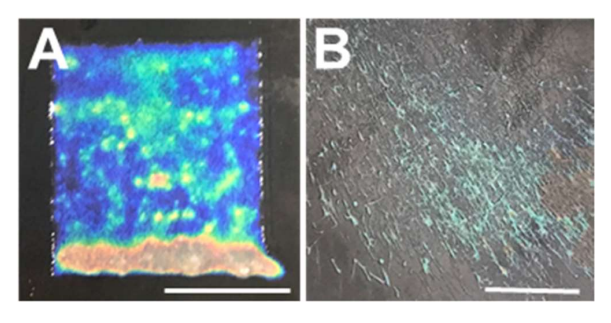


Figure 7. LC formulation tuned to show color at ambient conditions. (A) LC spread on a glass slide mounted on a black surface and (B) electrospun 10 wt % PCL fibers, 15 wt % LC fibers at ambient conditions (22 °C). Images captured with a smart phone; scale bar represents 1 cm.

attributed to the distribution in fiber size and fiber-to-fiber spacing affecting the apparent local temperature of the LC at ambient conditions. The thermochromic properties were observed as the ambient temperature fluctuated. Specifically, the fibers appeared blue at 73 °F/23 °C, green at 73 °F/23 °C, and red at 69 °F/21 °C (Figure S18). This dynamic response was observed over a much narrow temperature range than observed with cellulose-based liquid crystals; ⁸⁰ a green to orange transition was observed between 20 and 40 °C. Further characterizing the thermochromic properties of these fibers, e.g., red-end temperature below ambient temperature, may be useful as part of future studies. These results demonstrate that visually colored fibers can be achieved using this approach.

Overall, these results demonstrate that electrospinning PCL/LC blends can result in nonwoven products that visibly change color with temperature (captured with a video camera/smart phone). The dynamic properties can be tuned by varying the LC formulation and no crosslinking is required (a potential advantage as crosslinking can affect the reversibility of LC color change). Achieving responsive nonwoven products may enable products such as face masks for fever detection and are complementary to other approaches coating filament for woven products (100–300 μ m diameter), and extruding filament (500 μ m filament diameter) for three-dimensional (3D) printed parts and other applications.

■ CONCLUSIONS

Electrospun PS/LC and PCL/LC fibers without bead defects and nonwoven fiber mats have been achieved utilizing singleneedle blend electrospinning. Using electrospinnable polymer concentrations was necessary to produce LC-loaded fibers without bead defects. LC loadings (up to 60 wt % LC in PCL) were achieved without negatively impacting fiber morphology. Higher LC loadings were possible using PS (83 wt % LC in PS). Both fiber systems were temperature-responsive when observed under the PLM (i.e., single fiber analysis). Only the PCL fibers resulted in nonwoven materials that visibly changed color with temperature (captured with a video camera/smart phone). When selecting a polymer, fiber formation in a solvent that is miscible with the LC formulation and low glasstransition temperature appear to be important considerations for blend electrospinning. DSC and single fiber analysis indicate that the mesophase transition temperature and intrinsic pitch of the LC within a single fiber are not significantly affected by fiber processing and confinement within the fiber. Color analysis of the fiber mats indicates that layering of the fiber mat affects the structural color; the dynamic color is more noticeable (larger ΔE) and the "color play" is extended over larger temperature ranges than the LC alone. Colored fibers were achieved by tuning the transition temperature of the LC formulation. Such structurally colored, temperature-responsive nonwoven products may be useful for applications such as smart face masks.

ASSOCIATED CONTENT

Supporting Information

The Supporting Information is available free of charge at https://pubs.acs.org/doi/10.1021/acsapm.3c00222.

Additional experimental details and characterization data (PDF)

AUTHOR INFORMATION

Corresponding Author

Christina Tang — Chemical and Life Science Engineering, Virginia Commonwealth University, Richmond, Virginia 23284, United States; orcid.org/0000-0001-6204-0129; Email: ctang2@vcu.edu

Authors

Melissa W. Williams — Chemical and Life Science Engineering, Virginia Commonwealth University, Richmond, Virginia 23284, United States

James Aaron Wimberly — Chemical and Life Science Engineering, Virginia Commonwealth University, Richmond, Virginia 23284, United States

Ratib M. Stwodah — Chemical and Life Science Engineering, Virginia Commonwealth University, Richmond, Virginia 23284, United States

Jimmy Nguyen — Chemical and Life Science Engineering, Virginia Commonwealth University, Richmond, Virginia 23284, United States; orcid.org/0000-0002-3228-1711

Paola A. D'Angelo — U.S. Army Combat Capabilities Development Command Soldier Center, Natick, Massachusetts 01760, United States

Complete contact information is available at: https://pubs.acs.org/10.1021/acsapm.3c00222

Notes

The authors declare no competing financial interest.

ACKNOWLEDGMENTS

This work was partially supported by NSF (Award number 1651957) and Natick (grant nos. W911QY-17-2-0003 and W911QY-22-2-0002). The manuscript was approved for public release PAO number PR2023_62520.

■ REFERENCES

- (1) Liu, L.; Xu, W.; Ding, Y.; Agarwal, S.; Greiner, A.; Duan, G. A Review of Smart Electrospun Fibers toward Textiles. *Compos. Commun.* **2020**, 22, No. 100506.
- (2) Geng, Y.; Kizhakidathazhath, R.; Lagerwall, J. P. F. Robust Cholesteric Liquid Crystal Elastomer Fibres for Mechanochromic Textiles. *Nat. Mater.* **2022**, *21*, 1441–1447.
- (3) Wei, X.; Xue, Y.; Sun, Y.; Chen, L.; Zhang, C.; Wu, Q.; Peng, S.; Ma, C.; Liu, Z.; Jiang, S.; Yang, X.; Agarwal, S.; Duan, G. A Robust Anisotropic Light-Responsive Hydrogel for Ultrafast and Complex

- Biomimetic Actuation via Poly(Pyrrole)-Coated Electrospun Nanofiber. Chem. Eng. J. 2023, 452, No. 139373.
- (4) Wei, X.; Chen, L.; Wang, Y.; Sun, Y.; Ma, C.; Yang, X.; Jiang, S.; Duan, G. An Electrospinning Anisotropic Hydrogel with Remotely-Controlled Photo-Responsive Deformation and Long-Range Navigation for Synergist Actuation. *Chem. Eng. J.* 2022, 433, No. 134258.
- (5) Wang, H.; Zhang, Y.; Liang, X.; Zhang, Y. Smart Fibers and Textiles for Personal Health Management. ACS Nano 2021, 15, 12497–12508.
- (6) Guan, Y.; Agra-Kooijman, D. M.; Fu, S.; Jákli, A.; West, J. L. Responsive Liquid-Crystal-Clad Fibers for Advanced Textiles and Wearable Sensors. *Adv. Mater.* **2019**, *31*, No. 1902168.
- (7) Van Der Werff, L.; Kyratzis, I. L.; Robinson, A.; Cranston, R.; Peeters, G.; O'Shea, M.; Nichols, L. Thermochromic Composite Fibres Containing Liquid Crystals Formed via Melt Extrusion. *J. Mater. Sci.* **2013**, *48*, 5005–5011.
- (8) Xue, J.; Wu, T.; Dai, Y.; Xia, Y. Electrospinning and Electrospun Nanofibers: Methods, Materials, and Applications. *Chem. Rev.* **2019**, 119, 5298–5415.
- (9) Yang, X.; Wang, J.; Guo, H.; Liu, L.; Xu, W.; Duan, G. Structural Design toward Functional Materials by Electrospinning: A Review. *e-Polymers* **2020**, *20*, 682–712.
- (10) Yang, X.; Qi, H.; Jiang, S.; Dong, X.; Duan, G. Di-Aeolotropic Electric Conductive Janus Nanobelts with up-/down-Converting Fluorescence and Magnetism by Sequential Coaxial and Side-by-Side Electrospinning. *Compos. Commun.* **2022**, *35*, No. 101307.
- (11) Fadil, F.; Affandi, N. D. N.; Misnon, M. I.; Bonnia, N. N.; Harun, A. M.; Alam, M. K. Review on Electrospun Nanofiber-Applied Products. *Polymers* **2021**, *13*, No. 2087.
- (12) Zakrzewska, A.; Haghighat Bayan, M. A.; Nakielski, P.; Petronella, F.; De Sio, L.; Pierini, F. Nanotechnology Transition Roadmap toward Multifunctional Stimuli-Responsive Face Masks. ACS Appl. Mater. Interfaces 2022, 14, 46123—46144.
- (13) Cherrie, J. W.; Wang, S.; Mueller, W.; Wendelboe-Nelson, C.; Loh, M. In-Mask Temperature and Humidity Can Validate Respirator Wear-Time and Indicate Lung Health Status. *J. Exposure Sci. Environ. Epidemiol.* **2019**, 29, 578–583.
- (14) Kim, N.; Wei, J. L. J.; Ying, J.; Zhang, H.; Moon, S. K.; Choi, J. In *A Customized Smart Medical Mask for Healthcare Personnel*, International Conference on Industrial Engineering and Engineering Management (IEEM); IEEE, 2020; pp 581–585.
- (15) Miskovic, V.; Malafronte, E.; Minetti, C.; Machrafi, H.; Varon, C.; Iorio, C. S. Thermotropic Liquid Crystals for Temperature Mapping. Front. Bioeng. Biotechnol. 2022, 10, No. 806362.
- (16) White, T. J.; McConney, M. E.; Bunning, T. J. Dynamic Color in Stimuli-Responsive Cholesteric Liquid Crystals. *J. Mater. Chem.* **2010**, *20*, 9832–9847.
- (17) van der Werff, L. C.; Robinson, A. J.; Kyratzis, I. L. Combinatorial Approach for the Rapid Determination of Thermochromic Behavior of Binary and Ternary Cholesteric Liquid Crystalline Mixtures. ACS Comb. Sci. 2012, 14, 605–612.
- (18) Sage, I. Thermochromic Liquid Crystals. Liq. Cryst. 2011, 38, 1551–1561.
- (19) Kim, D. K.; Hwang, M.; Lagerwall, J. P. F. Liquid Crystal Functionalization of Electrospun Polymer Fibers. *J. Polym. Sci., Part B: Polym. Phys.* **2013**, *51*, 855–867.
- (20) Singh, U.; Mohan, S.; Davis, F. Selective Bragg Reflection of Visible Light from Coaxial Electrospun Fiber Mats. *J. Appl. Polym. Sci.* **2021**, *138*, No. 49647.
- (21) Wang, J.; Jákli, A.; West, J. L. Liquid Crystal/Polymer Fiber Mats as Sensitive Chemical Sensors. J. Mol. Liq. 2018, 267, 490–495.
- (22) Reyes, C. G.; Sharma, A.; Lagerwall, J. P. F. Non-Electronic Gas Sensors from Electrospun Mats of Liquid Crystal Core Fibres for Detecting Volatile Organic Compounds at Room Temperature. *Liq. Cryst.* **2016**, *43*, 1986–2001.
- (23) Schelski, K.; Reyes, C. G.; Pschyklenk, L.; Kaul, P. M.; Lagerwall, J. P. F. Quantitative Volatile Organic Compound Sensing with Liquid Crystal Core Fibers. *Cell Rep. Phys. Sci.* **2021**, 2, No. 100661.

- (24) Bertocchi, M. J.; Ratchford, D. C.; Casalini, R.; Wynne, J. H.; Lundin, J. G. Electrospun Polymer Fibers Containing a Liquid Crystal Core: Insights into Semiflexible Confinement. *J. Phys. Chem. C* **2018**, 122, 16964–16971.
- (25) Dicker, K. T.; Ratchford, D.; Casalini, R.; Thum, M. D.; Wynne, J. H.; Lundin, J. G. Surfactant Modulated Phase Transitions of Liquid Crystals Confined in Electrospun Coaxial Fibers. *Langmuir* **2020**, *36*, 7916–7924.
- (26) Thum, M. D.; Kolacz, J.; Ratchford, D. C.; Camarella, G.; Maza, W.; Lundin, J. G. Dynamic Interference Colors in Electrospun Microfibrous Mats. *Adv. Opt. Mater.* **2022**, *10*, No. 2200192.
- (27) Lagerwall, J. P. F.; McCann, J. T.; Formo, E.; et al. Coaxial Electrospinning of Microfibres with Liquid Crystal in the Core. *Chem. Commun.* **2008**, 2008, 5420–5422.
- (28) Enz, E.; Baumeister, U.; Lagerwall, J. Coaxial Electrospinning of Liquid Crystal-Containing Poly(Vinylpyrrolidone) Microfibres. *Beilstein J. Org. Chem.* **2009**, *5*, No. 58.
- (29) Enz, E.; La Ferrara, V.; Scalia, G. Confinement-Sensitive Optical Response of Cholesteric Liquid Crystals in Electrospun Fibers. ACS Nano 2013, 7, 6627–6635.
- (30) Nguyen, J.; Stwodah, R. M.; Vasey, C. L.; Rabatin, B. E.; Atherton, B.; D'Angelo, P. A.; Swana, K. W.; Tang, C.; D'Angelo, P. A.; Swana, K. W.; Tang, C. Thermochromic Fibers via Electrospinning. *Polymers* **2020**, *12*, No. 842.
- (31) Han, D.; Steckl, A. J. Coaxial Electrospinning Formation of Complex Polymer Fibers and Their Applications. *ChemPlusChem* **2019**, 84, 1453–1497.
- (32) Buzgo, M.; Mickova, A.; Rampichova, M.; Doupnik, M. Blend Electrospinning, Coaxial Electrospinning, and Emulsion Electrospinning Techniques. In Core-Shell Nanostructures for Drug Delivery and Theranostics: Challenges, Strategies and Prospects for Novel Carrier Systems; Focarete, M. L.; Tampieri, A., Eds.; Woodhead Publishing, 2018; pp 325–347.
- (33) Shankar, A.; Pal, S.; Srivastava, R.; Nandan, B. Phase Transitions of Liquid Crystal Confined in Electrospun Polymer Nanofibres. *Bull. Mater. Sci.* 2020, 43, No. 176.
- (34) Buyuktanir, E. A.; West, J. L.; Frey, M. W. In Optically Responsive Liquid Crystal Microfibers for Display and Nondisplay Applications, SPIE Proceedings, Emerging Liquid Crystal Technologies VI; SPIE, 2011; p 79550P.
- (35) Mamuk, A. E.; Koçak, Ç.; Aslan, S.; Altuntaş, D. B. Electrochemical Properties of Coumarin 500 Encapsulated in a Liquid Crystal Guided Electrospun Fiber Core and Their Supercapacitor Application. ACS Appl. Energy Mater. 2022, 5, 12078—12089.
- (36) Koçak, Ç.; Mamuk, A. E.; Dönmez, Ç. E. D.; Poyraz, M. Electrospun Fibers of Liquid Crystal Mixtures. J. Mater. Sci.: Mater. Electron. 2022, 33, 15209–15221.
- (37) Deng, X.; Zhao, Y.; Gao, H.; Wang, D.; Miao, Z.; Cao, H.; Yang, Z.; He, W. Thermally Bandwidth-Controllable Reflective Liquid Crystal Films Prepared by Doping Nano-Sized Electrospun Fibers. *Liq. Cryst.* **2021**, 48, 1525–1533.
- (38) Nasajpour, A.; Mostafavi, A.; Chlanda, A.; Rinoldi, C.; Sharifi, S.; Ji, M. S.; Ye, M.; Jonas, S. J.; Swieszkowski, W.; Weiss, P. S.; Khademhosseini, A.; Tamayol, A. Cholesteryl Ester Liquid Crystal Nanofibers for Tissue Engineering Applications. *ACS Mater. Lett.* **2020**, *2*, 1067–1073.
- (39) Levit, S. L.; Nguyen, J.; Hattrup, N. P.; Rabatin, B. E.; Stwodah, R.; Vasey, C. L.; Zeevi, M. P.; Gillard, M.; Angelo, P. A. D.; Swana, K. W.; Tang, C. Color Space Transformation-Based Algorithm for Evaluation of Thermochromic Behavior of Cholesteric Liquid Crystals Using Polarized Light Microscopy. ACS Omega 2020, 5, 7149—7157.
- (40) Zheng, T.; Zhou, Q.; Li, Q.; Li, H.; Zhang, L.; Hu, Y. Application of Successive Self-Nucleation and Annealing (SSA) to Poly(1-Butene) Prepared by Ziegler-Natta Catalysts with Different External Donors. *RSC Adv.* **2015**, *5*, 9328–9336.
- (41) Kuo, S. W.; Huang, C. F.; Chang, F. C. Study of Hydrogen-Bonding Strength in Poly(ε -Caprolactone) Blends by DSC and FTIR. *J. Polym. Sci., Part B: Polym. Phys.* **2001**, *39*, 1348–1359.

- (42) Feng, L.; Bian, X.; Li, G.; Chen, Z.; Cui, Y.; Chen, X. Determination of Ultra-Low Glass Transition Temperature via Differential Scanning Calorimetry. *Polym. Test.* **2013**, 32, 1368–1372.
- (43) Plata, G. J. D.; delos Santos, R. M. Application of Image Processing Programs in Color Analysis of Wood Photodegradation. *J. Phys.: Conf. Ser.* **2022**, 2288, No. 012003.
- (44) Smith, T.; Guild, J. The C.I.E. Colorimetric Standards and Their Use. Trans. Opt. Soc. 1932, 33, 73–134.
- (45) Yang, R.; Cheng, W.; Chen, X.; Qian, Q.; Zhang, Q.; Pan, Y.; Duan, P.; Miao, P. Color Space Transformation-Based Smartphone Algorithm for Colorimetric Urinalysis. *ACS Omega* **2018**, *3*, 12141–12146.
- (46) Wu, A.; Beck, C.; Ying, Y.; Federici, J.; Iqbal, Z. Thermochromism in Polydiacetylene-ZnO Nanocomposites. *J. Phys. Chem. C* **2013**, *117*, 19593–19600.
- (47) Bonino, C. A.; Krebs, M. D.; Saquing, C. D.; Jeong, S. I.; Shearer, K. L.; Alsberg, E.; Khan, S. A. Electrospinning Alginate-Based Nanofibers: From Blends to Crosslinked Low Molecular Weight Alginate-Only Systems. *Carbohydr. Polym.* **2011**, *85*, 111–119.
- (48) Yao, K.; Chen, J.; Li, P.; Duan, G.; Hou, H. Robust Strong Electrospun Polyimide Composite Nanofibers from a Ternary Polyamic Acid Blend. *Compos. Commun.* **2019**, *15*, 92–95.
- (49) Van der Schueren, L.; De Schoenmaker, B.; Kalaoglu, Ö. I.; De Clerck, K. An Alternative Solvent System for the Steady State Electrospinning of Polycaprolactone. *Eur. Polym. J.* **2011**, 47, 1256—1263.
- (50) Jarusuwannapoom, T.; Hongrojjanawiwat, W.; Jitjaicham, S.; Wannatong, L.; Nithitanakul, M.; Pattamaprom, C.; Koombhongse, P.; Rangkupan, R.; Supaphol, P. Effect of Solvents on Electro-Spinnability of Polystyrene Solutions and Morphological Appearance of Resulting Electrospun Polystyrene Fibers. Eur. Polym. J. 2005, 41, 409–421.
- (51) Acosta, M.; Santiago, M. D.; Irvin, J. A. Electrospun Conducting Polymers: Approaches and Applications. *Materials* **2022**, *15*, No. 8820.
- (52) Ewaldz, E.; Brettmann, B. Molecular Interactions in Electrospinning: From Polymer Mixtures to Supramolecular Assemblies. ACS Appl. Polym. Mater. 2019, 1, 298–308.
- (53) Shenoy, S. L.; Bates, W. D.; Frisch, H. L.; Wnek, G. E. Role of Chain Entanglements on Fiber Formation during Electrospinning of Polymer Solutions: Good Solvent, Non-Specific Polymer-Polymer Interaction Limit. *Polymer* 2005, 46, 3372–3384.
- (54) McKee, M. G.; Wilkes, G. L.; Colby, R. H.; Long, T. E. Correlations of Solution Rheology with Electrospun Fiber Formation of Linear and Branched Polyesters. *Macromolecules* **2004**, *37*, 1760–1767.
- (55) Elzein, T.; Nasser-Eddine, M.; Delaite, C.; Bistac, S.; Dumas, P. FTIR Study of Polycaprolactone Chain Organization at Interfaces. *J. Colloid Interface Sci.* **2004**, 273, 381—387.
- (56) Lin, S. Y.; Li, M. J.; Lin, H. L. Effect of Skin-Penetrating Enhancers on the Thermophysical Properties of Cholesteryl Oleyl Carbonate Embedded in a Thermo-Responsive Membrane. *J. Mater. Sci.: Mater. Med.* **2000**, *11*, 701–704.
- (57) Wang, J.; Cheung, M. K.; Mi, Y. Miscibility and Morphology in Crystalline/Amorphous Blends of Poly (Caprolactone)/Poly(4-Vinylphenol) as Studied by DSC, FTIR, and 13C Solid State NMR. *Polymer* **2002**, *43*, 1357–1364.
- (58) Gupta, S. J.; Balakrishna, R. S.; Vinita, D. In *Investigation of Parameters of Liquid Crystal Mixtures*, Proceedings of the International Conference & Workshop on Emerging Trends in Technology ICWET '11; Association for Computing Machinery: 2011; pp 1088–1094.
- (59) Islam, M. S.; Yeum, J. H.; Das, A. K. Effect of Pullulan/Poly(Vinyl Alcohol) Blend System on the Montmorillonite Structure with Property Characterization of Electrospun Pullulan/Poly(Vinyl Alcohol)/Montmorillonite Nanofibers. *J. Colloid Interface Sci.* **2012**, 368, 273–281.
- (60) Samanta, A.; Takkar, S.; Kulshreshtha, R.; Nandan, B.; Srivastava, R. K. Facile Fabrication of Composite Electrospun

- Nanofibrous Matrices of Poly(ε-Caprolactone)-Silica Based Pickering Emulsion. *Langmuir* **2017**, *33*, 8062–8069.
- (61) Yang, Z.; Peng, H.; Wang, W.; Liu, T. Crystallization Behavior of Poly(ε -Caprolactone)/Layered Double Hydroxide Nanocomposites. *J. Appl. Polym. Sci.* **2010**, *116*, 2658–2667.
- (62) Enz, E.; Lagerwall, J. Electrospun Microfibres with Temperature Sensitive Iridescence from Encapsulated Cholesteric Liquid Crystal. J. Mater. Chem. 2010, 20, 6866–6972.
- (63) Wei, M.; Kang, B.; Sung, C.; Mead, J. Core-Sheath Structure in Electrospun Nanofibers from Polymer Blends. *Macromol. Mater. Eng.* **2006**, *291*, 1307–1314.
- (64) Li, S.; Li, Y.; Qian, K.; Ji, S.; Luo, H.; Gao, Y.; Jin, P. Functional Fiber Mats with Tunable Diffuse Reflectance Composed of Electrospun VO2/PVP Composite Fibers. ACS Appl. Mater. Interfaces 2014, 6, 9–13.
- (65) Li, X.; Zhou, J.; Quan, Z.; Wang, L.; Li, F.; Qin, X.; Yu, J. Light Scattering Tunability of Nanofiber Membrane for Enhancing Color Yield. *Dyes Pigm.* **2021**, *193*, No. 109462.
- (66) Greene, J. P. Automotive Plastics and Composites: Materials and Processing; Ebnesajjad, S., Ed.; William Andrew: Oxford, UK, 2021.
 (67) Ebnesajjad, S. Plastic Films in Food Packaging: Materials, Technology and Applications; William Andrew: Oxford, UK, 2013.
- (68) Lee, S. W.; Yoon, J.; Kim, H. C.; Lee, B.; Chang, T.; Ree, M. Effect of Molecular Weight on the Surface Morphology, Molecular Reorientation, and Liquid Crystal Alignment Properties of Rubbed Polystyrene Films. *Macromolecules* **2003**, *36*, 9905–9916.
- (69) Honaker, L. W.; Vats, S.; Anyfantakis, M.; Lagerwall, J. P. F. Elastic Sheath-Liquid Crystal Core Fibres Achieved by Microfluidic Wet Spinning. J. Mater. Chem. C 2019, 7, 11588–11596.
- (70) Huang, X.-Y.; Khan, A. A.; Davis, D. J.; Podojil, G. M.; Jones, C. M.; Miller, N.; Doane, J. W. In *Color Reflective Cholesteric Liquid Crystal Display*, SPIE Proceedings, Liquid Crystal Materials, Devices, and Applications VII; SPIE, 1999.
- (71) Mitov, M. Cholesteric Liquid Crystals in Living Matter. Soft Matter 2017, 13, 4176–4209.
- (72) Badran, H. A.; Bader, S. J.; Alfahed, R. K. F.; Saleh, N. A.-H. Study of Colorimetric Properties of Ethidium Bromide Dye-Doped PVP/DNA Film. *J. Phys.: Conf. Ser.* **2021**, *1963*, No. 012102.
- (73) Zhou, H.; Wang, H.; He, W.; Yang, Z.; Cao, H.; Wang, D.; Li, Y. Research Progress of Cholesteric Liquid Crystals with Broadband Reflection. *Molecules* **2022**, *27*, No. 4427.
- (74) Choi, H.; Kim, J.; Nishimura, S.; Toyooka, T.; Araoka, F.; Ishikawa, K.; Wu, J. W.; Takezoe, H. Broadband Cavity-Mode Lasing from Dye-Doped Nematic Liquid Crystals Sandwiched by Broadband Cholesteric Liquid Crystal Bragg Reflectors. *Adv. Mater.* **2010**, 22, 2680–2684.
- (75) Huang, Y.; Zhou, Y.; Wu, S.-T. Broadband Circular Polarizer Using Stacked Chiral Polymer Films. *Opt. Express* **2007**, *15*, No. 6414. (76) Jewell, S. A.; Vukusic, P.; Roberts, N. W. Circularly Polarized Colour Reflection from Helicoidal Structures in the Beetle Plusiotis Boucardi. *New J. Phys.* **2007**, *9*, No. 99.
- (77) Borrotti, M.; Lanzarone, E.; Manganini, F.; Ortelli, S.; Pievatolo, A.; Tonetti, C. Defect Minimization and Feature Control in Electrospinning through Design of Experiments. *J. Appl. Polym. Sci.* **2017**, *134*, No. 44740.
- (78) Ruiter, F. A. A.; Alexander, C.; Rose, F. R. A. J.; Segal, J. I. A Design of Experiments Approach to Identify the Influencing Parameters That Determine Poly-D,L-Lactic Acid (PDLLA) Electrospun Scaffold Morphologies. *Biomed. Mater.* **2017**, *12*, No. 055009.
- (79) Hakami, A.; Srinivasan, S. S.; Biswas, P. K.; Krishnegowda, A.; Wallen, S. L.; Stefanakos, E. K. Review on Thermochromic Materials: Development, Characterization, and Applications. *J. Coat. Technol. Res.* **2022**, 19, 377–402.
- (80) Zhang, Z.; Wang, C.; Wang, Q.; Zhao, Y.; Shang, L. Cholesteric Cellulose Liquid Crystal Ink for Three-Dimensional Structural Coloration. *Proc. Natl. Acad. Sci. U.S.A.* **2022**, *119*, No. e2204113119. (81) Yuan, W.; Zhou, N.; Shi, L.; Zhang, K.-Q. Structural Coloration of Colloidal Fiber by Photonic Band Gap and Resonant Mie Scattering. *ACS Appl. Mater. Interfaces* **2015**, *7*, 14064–14071.

(82) Chan, C. L. C.; Lei, I. M.; van de Kerkhof, G. T.; Parker, R. M.; Richards, K. D.; Evans, R. C.; Huang, Y. Y. S.; Vignolini, S. 3D Printing of Liquid Crystalline Hydroxypropyl Cellulose—toward Tunable and Sustainable Volumetric Photonic Structures. Adv. Funct. Mater. 2022, 32, No. 2108566.



Nonconventional Fluorescence-Based Circularly Polarized **Luminescent Core/Shell Particles: Maleic Anhydride** Copolymer as the Core and Chiral Helical Polyacetylene a...

Yanze Liu, Jianping Deng, et al.

APRIL 06, 2023 ACS MACRO LETTERS

READ 🗹

Tough and Transparent Photonic Hydrogel Nanocomposites for Display, Sensing, and Actuation Applications

Liqian Zhu, Yongqing Xia, et al.

APRIL 17, 2023

ACS APPLIED NANO MATERIALS

READ 🗹

Integrated Thermoelectric Design Inspired by Ionic Liquid Microemulsion-Based Gel with Regulatable Dual-**Temperature Responsiveness**

Yuzhen Qian, Jingcheng Hao, et al.

MARCH 30, 2023

ACS APPLIED POLYMER MATERIALS

READ 🗹

Nature-Inspired Heat and Moisture Exchanger Filters Composed of Gelatin and Chitosan for the Design of Eco-Sustainable "Artificial Noses"

Elisabetta Campodoni, Monica Sandri, et al.

APRIL 12, 2023 ACS APPLIED POLYMER MATERIALS

READ 🗹

Get More Suggestions >